Wear Performance of Incoloy 800HT and Inconel 617 in Various Surface Conditions for High-Temperature Gas-Cooled Reactor Components

Valentin Pauly[a], Joseph Kern[a], Malcolm Clark[a], David S. Grierson[a], Kumar Sridharan[a]*

[a]*University of Wisconsin-Madison, Room 919, 1500 Engineering Drive, Madison, WI 53706, USA*
**Corresponding author kumar.sridharan@wisc.edu*

Abstract

Incoloy™ 800HT and Inconel™ 617 are primary candidate structural materials for high-temperature gas-cooled reactors (HTGRs). Impurities (e.g., H_2O, CH_4) in the coolant induce corrosion reactions that affect tribological behavior. We investigate the high-temperature tribological performance of the alloys under surface conditions including: conditioned in H_2O-containing helium at elevated temperatures, hardened via the carbon-diffusion Kolsterising® treatment, and conditioned after hardening. Initial friction coefficients and volume removed serve as metrics for wear performance. We find that wear mechanisms including scuffing, glaze-oxide formation, and oxide-layer wear and break-through are governed by surface hardness, chemistry, and applied load. The formation of a glaze-oxide layer is achieved with an oxide of sufficient mechanical integrity if the oxide-substrate interface is strong and the load is low.

Keywords: Wear, Friction, High Temperature, Scuffing

1. INTRODUCTION

Generation IV High-Temperature Gas-cooled Reactors (HTGRs) are being designed to generate electricity at efficiencies that exceed those of the present light-water reactors (LWRs) and also be a source of process heat for a range of industrial applications [1]. To increase efficiency, temperatures exceeding 750 °C will be required, and the reactors are being engineered to reach 60-year operational lifetimes. These two constraints require the use of structural materials with exceptional high-temperature strength and resistance to corrosion. Incoloy™ 800HT and Inconel™ 617 are superalloy candidate materials that have been selected for structural applications in HTGRs based on their ASME code certification. A number of experimental studies have been performed to demonstrate the exceptional strength and toughness of these alloys under a range of environments that are relevant to HTGR operation [2–8].

Helium, the primary coolant in HTGRs, will contain a number of impurities, including H_2, H_2O, CO_2, CO, and CH_4. Exposure to trace levels of these impurities will induce corrosion reactions that could degrade the integrity of the structural materials. In addition, components including valves, valve seats, and valve shafts that will experience contact and sliding stresses as well as corrosion will undergo a combination of chemical modification and mechanical wear, both of which can lead to decreased lifetimes of the components and downtime for the reactor. Wear of corroded components can lead to dimensional changes, wear-debris generation, and self-welding, all of which can cause component seizure and/or failure. A combined understanding of the corrosion and wear mechanisms for candidate alloys under prototypical HTGR conditions is therefore needed in order to develop the engineering solutions to actualize desired reactor lifecycles.

Coatings and surface treatments to improve hardness and wear resistance are applied in a wide range of industries to protect the underlying substrate material from damage or alteration [9]. They can be used to close the gap in hardness between the substrate and a potential external oxide layer or subsequent coating, thereby improving the strength and integrity of the component [10,11]. In particular, surface treatments/modifications of superalloys by diffusion processes have received considerable attention for improving corrosion and wear properties [12]. Kolsterising® is a carbon diffusion process which enhances the surface mechanical properties of austenitic stainless steel and nickel-based alloys. Carburizing is one of the most widely used surface hardening techniques [13]. As a result, the surface gets harder which may lead to an increase in galling, erosion and fretting wear resistance, and increase in fatigue life [14]. The diffusion layer can reach a depth up to 50µm, and since the process is conducted at low temperature, the formation of carbides is suppressed, and the corrosion resistance should be preserved [15]. Kolsterising® is also attractive for tribological applications because there is no sharp interface (as in an overlay coating) and delamination of the surface is a non-issue [15].

Here we report the results from analyzing the surface composition, surface morphology, and the tribological behavior of as-received and Kolsterised alloys 800HT and 617 in the presence of trace levels of oxygen-bearing impurities at high temperatures. The surfaces of both alloys were characterized after extended high-temperature exposure to impure helium with 4 ppmv H_2O - 750 °C for alloy 800HT, and 900 °C for alloy 617. Ex-situ pin-on-disk tribology tests were performed at elevated temperatures in an ambient air environment – either 650 °C or 750 °C for alloy 800HT, and either 850 °C or 900 °C for alloy 617. Surface characterization and tribological measurements are reported for the two alloys in their as-received condition, after high-temperature exposure to impure helium, after Kolsterising®, and after Kolsterising® followed by high-temperature exposure to impure helium. Results from non-Kolsterised as-received and conditioned samples from our previously published study [16] are shown to provide a baseline reference for evaluating the effects of the Kolsterising® process.

2. EXPERIMENTAL PROCEDURE

2.1. Materials

Table 1: Nominal compositions of alloys 800HT and 617 used in this study (wt.%).

Element	Fe	Ni	Cr	Mn	C	Cu	Si	S	Al	Ti	Al+Ti	Mo	Co
800HT	45.8	31.4	19.7	1.01	0.066	0.25	0.25	0.001	0.43	0.54	0.97	/	/
617	1.6	54.1	22.2	0.1	0.05	0.04	0.1	<0.002	1.1	0.4	1.5	8.6	11.6

Incoloy™ 800HT and Inconel™ 617 are ASME-certified materials (UNS N08811, ASTM B408-06, ASME SB408 standards for 800HT and UNS N06617, ASTM B168-08, ASME SB168 standards for 617). Table 1 shows the compositions (wt %) of the samples used for this work. Details regarding material procurement, machining, and polishing of the pins and disks can be found in our previously published work [16]. Disks were 2” in diameter and ¼” in thickness, and pins were machined to radii of 16.3 mm, 55.3mm, or 255.4 mm. Disks and pins were cleaned ultrasonically in acetone and rinsed with DI water prior to conditioning, Kolsterising®, and testing.

2.2. Kolsterising®

Carburization of the samples was achieved via the commercial Kolsterising® process by Bodycote. Kolsterising® is a low temperature process (< 500 °C). Due to the low process temperature, the formation of chromium carbides is suppressed thereby preserving the chromium oxide passive surface layer that provides the corrosion resistance to these systems. Carbon is interstitially dissolved in the lattice resulting in a supersaturation of carbon in the alloy. The Kolsterising® treatment is applicable to nearly all austenitic and duplex stainless steels, Ni-base and Co-Cr alloys [15]. Surface hardnesses of greater than 1000 HV can be achieved in most common austenitic and duplex stainless steels and Ni-based and Co-Cr alloys. Case depths typically range from 10-40 μm.

2.3. Conditioning

Conditioning of the samples was achieved by exposing them to helium containing trace levels of impurities at elevated temperatures for extended periods of time. A once-through helium flow loop was used to oxidize the pins and disks by subjecting them to a continuous flow of impure helium with 4 ppmv H_2O. Oxygen-bearing impurities at ppm levels are known to induce corrosion reactions at high temperatures and are representative of the concentrations expected in HTGRs [5]. Additional details regarding the helium loop can be found in our earlier paper [16]. Alloy 800HT was conditioned at 750 °C for 22 days, while alloy 617 was conditioned at 900 °C for 22 days. Henceforth the descriptors “conditioned” and “conditioning” will refer to these two conditions for the respective alloys.

2.4. *Tribological testing*

Tribological testing was performed using a pin-on-disk THT high-temperature tribometer (CSM Instruments SA, now Anton Paar GmbH) at temperatures up to 900 °C. The load, the temperature, and the speed of disk rotation can be adjusted by the user. The friction force and the sliding distance are recorded throughout the duration of the test. Tribological testing of both alloys was performed in ambient air for 1 hour per test at a sliding speed of 10 cm/s - alloy 800HT was tested at either 650 °C or 750 °C, and alloy 617 was tested at either 850 °C or 900 °C. All wear tests discussed here achieved steady-state sliding before the tests were terminated. The total number of cycles varied from 2,992 to 12,012 depending on the radius of the wear track (between 4.77 mm and 19.15 mm). 1N, 2N, and 5 N load levels were applied using pins with radii of 16.3 mm, 55.3 mm, and 255.4 mm, respectively, to reach initial mean contact stresses of ~120 MPa, ~65 MPa, and ~30 MPa, respectively. Samples were allowed to cool passively after completion of the tribotest. Initial friction coefficients were obtained by averaging the values of the friction coefficient over the first ten cycles. Steady-state friction coefficients were obtained by averaging the friction coefficient over the steady-state portion of the test. The friction values provided information regarding the resistance to sliding at the initial stages of wear and after the contact stabilized, respectively. Evaluation of the friction curves also enabled quantification of the time required for the tribosystem to run in. Wear volumes and initial friction coefficient values are reported here as a function of the sample-treatment and tribotesting conditions to investigate correlations between the measured quantities and the wear mechanisms.

2.5. Characterization

Scanning electron microscopy (SEM) equipped with electron dispersion spectroscopy (EDS) (Carl Zeiss AG) was used to obtain cross-sectional views of the samples before and after conditioning and Kolsterising®. SEM-EDS was also used to obtain plan-view images and chemical maps of the samples after tribological testing. A TI 950 TriboIndenter (Hysitron, Inc.) with a diamond Berkovich tip was used to quantify nanohardness of the as-received samples and the worn surfaces of the conditioned samples. The area function of the Berkovich tip was calibrated with a quartz reference to ensure <10% accuracy of the hardness results. Glow-discharge optical emission spectroscopy (GDOES) was performed on the candidate alloys using a Horiba GD Profiler-2 to quantify the elemental composition as a function of depth down to 50 µm below the surface. GDOES measurements were performed at 700 Pa and 40 W, with an average sputter rate of 0.0783 ± 0.060 µm/s for 800HT and 0.0957 ± 0.0018 µm/s for 617, respectively. X-Ray Diffraction (XRD) (Bruker D8 Discover) was used to identify the phases on the surfaces of samples. Scanning white-light interferometry (Zygo Corporation) was used to quantify worn volumes of the wear tracks formed on the disks after pin-on-disk tribotesting as it offers accurate and high-resolution 2D maps for quantifying surface modification due to wear [17]. Prior to imaging with the interferometer, the samples were sputter coated with a ~50-nm thick Au layer to render the surfaces reflective without affecting the worn-volume calculations. Values for the wear volume were determined by selecting two locations on the wear track of the disk quantifying the volume of material removed from those locations (i.e., the volume of material missing below the surface plane of the disk), averaging those volumes, and then extrapolating that average volume across the total circumference of the wear track. Worn volumes reported here are normalized by the circumference of the wear track (V/C) to adjusting values measured from different track radii to a common scale. The uncertainty in the worn volumes was computed via uncertainty propagation considering the following: the uncertainty in the measured track radius (±0.515 mm), the standard deviation due to the number of measurements obtained from different regions, and the uncertainty in the measurement technique itself. Uncertainty in measurement was determined by quantifying the volume of material lying below the background

plane of an unworn sample. The numerical value of the uncertainty quantifies the worn volume below which wear is indistinguishable from the roughness of an unworn region.

3. RESULTS

Alloys 800HT and 617 were tribotested as-received, after conditioning, after Kolsterising®, and after Kolsterising® followed by conditioning. All tribological testing was performed via pin-on-disk wear testing at elevated temperatures in ambient air environments.

3.1. Alloy 800HT

3.1.1. As-received and conditioned samples

This section will provide the results on the corrosion of alloy 800HT in a HTGR-like environment and the impact of corrosion on the high-temperature tribological behavior.

3.1.1.1. Corrosion results

Figure 1 shows the cross-sectional SEM micrograph and EDS line scan of conditioned alloy 800HT. The cross-sectional SEM micrograph and EDS line scan of as-received alloy 800HT is provided in Figure S1 of the supplemental material as a baseline reference. Figure 1 (a) indicates that a uniform oxide layer formed across the surface, with a total thickness of the layer measuring 1.33 ± 0.44 µm. The composition profile exhibits oxidation in the form of a slightly manganese-enriched external chromium oxide. In addition, Figure 1 (b) shows the presence of an aluminum oxide beneath the surface oxide. That sub-surface aluminum-oxide region developed along a grain boundary due to aluminum that segregated to the grain boundaries and combined with oxygen that diffused into the sample. In Figure 1 (b), the grain boundary oxide is measured between 2 and 4 µm from the surface.

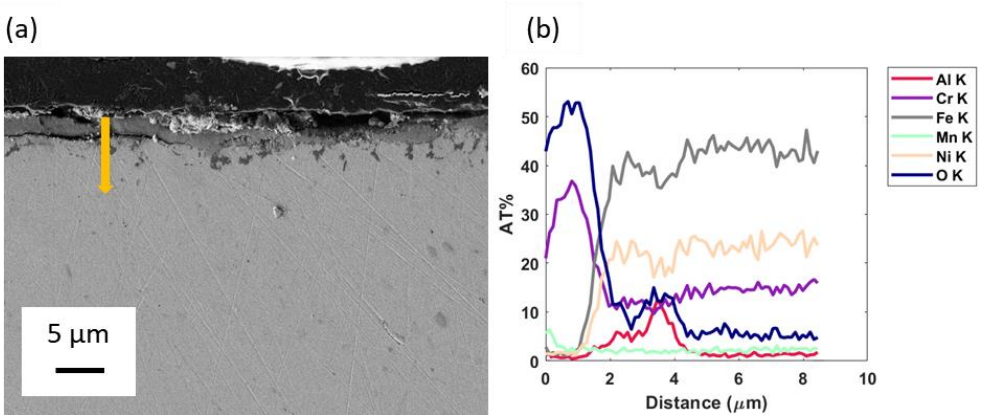

Figure 1: (a) Cross-sectional SEM image and (b) EDS line scan of conditioned alloy 800HT.

3.1.1.2. Tribological results

The wear volumes for as-received and conditioned alloy 800HT are shown in Figure 2 (a, b) as a function of load and initial friction coefficient, respectively. The applied loads were precisely 1, 2 or 5 N, but the abscissas of the data points in Figure 2 (a) are shifted slightly for clarity. In the wear-volume plots, the sizes of the symbols are proportional to the load applied during the tribotests. In Figure 2 (a), the testing temperatures during the tribotests are displayed in the legend. In Figure 2 (b), the data acquired at the

two different temperature levels are combined due to the absence of a trend among those levels. This plotting format will be employed for the remainder of the paper. To enhance data visualization, 3D rotational versions of the wear-volume plots are available online as interactive plots. Firstly, it can be inferred that the testing temperature over this range does not have a measurable impact on the tribological behavior of alloy 800HT. As confirmed by Rahman et al. in [18], for as-received alloy 800HT, the wear volume and the associated uncertainty increase with increasing load. Most of the conditioned samples exhibit wear volumes below the detection threshold of the measurement technique. Conditioned alloy 800HT only experiences measurable wear in some cases under a 5N load, indicating a threshold around 5N at or above which significant wear can occur. Figure 2 (b) shows the strong correlation between initial friction coefficient and wear volume, whereby negligible wear (V/C < 1 $\mu m^3/mm$) occurs when the initial friction coefficient is smaller (~0.5), and measurable wear (V/C > 10 $\mu m^3/mm$) occurs when the initial friction coefficient is larger (~1). The two distinct data clusters in Figure 2 (b) suggest that two different wear mechanisms are at play. Subsequent characterization results will elucidate the mechanisms.

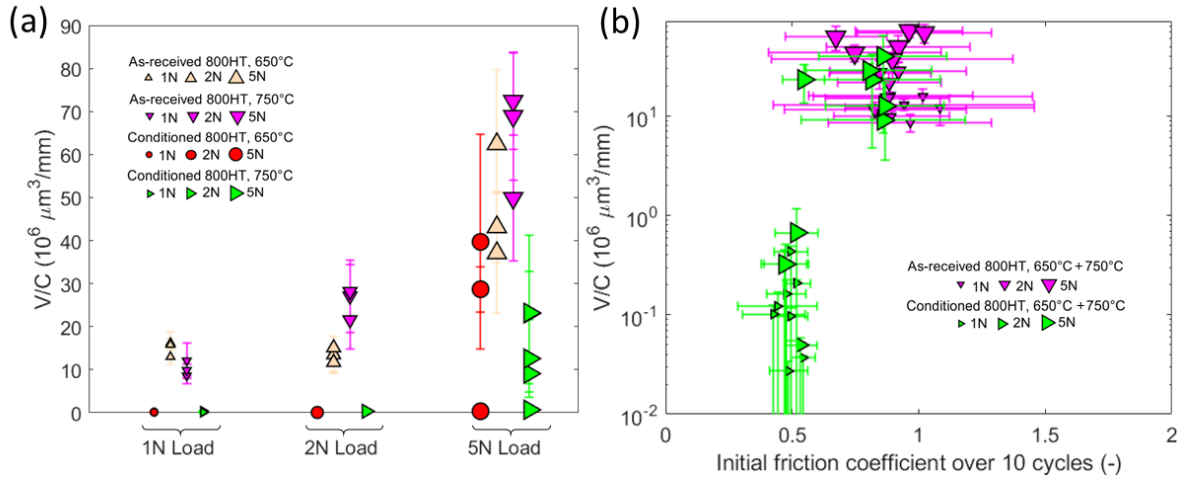

Figure 2: Wear volumes as a function of (a) load and (b) initial friction coefficient for as-received alloy 800HT and conditioned alloy 800HT. The temperature during wear testing is stated in the legend labels. A 3D rotational version of these data is available as an interactive plot.

SEM micrographs of the wear tracks for as-received alloy 800HT are shown in Figure 3 (a-d). The wear is dominated by scuffing and gouging at both loads, and no evidence of oxide compaction is visible. Figure 3 (c) indicates a wider wear track for the 5N-load test compared to the 1N-load test on Figure 3 (a).

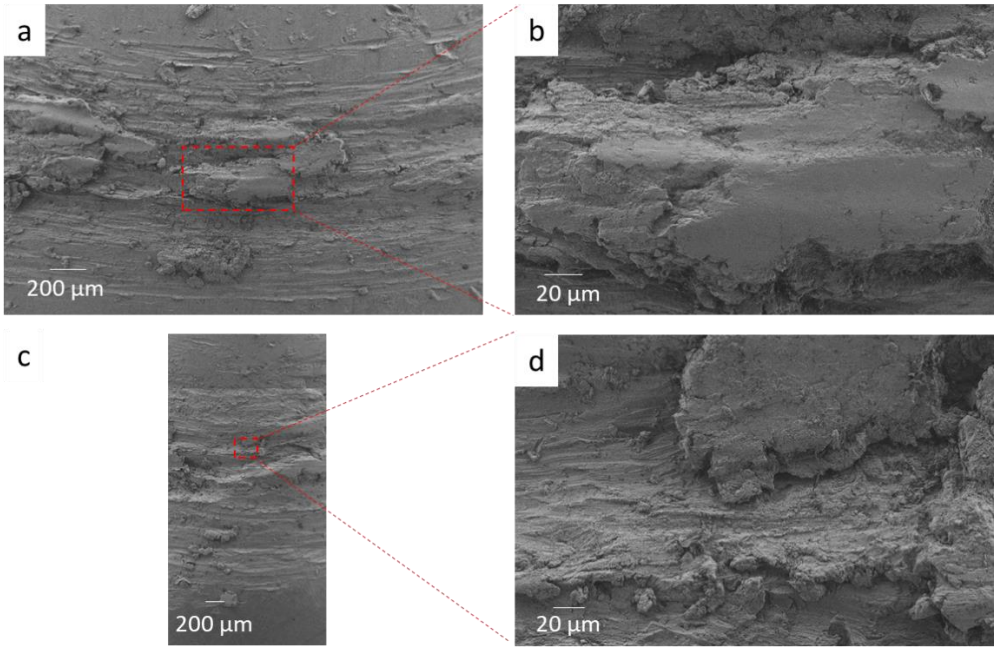

Figure 3: Morphology of the wear tracks for as-received alloy 800HT after wear testing at 750 °C under (a, b) 1N load and (c, d) 5N load [16].

The compositions of the wear track and of the unworn surface for as-received alloy 800HT are shown in the plan-view EDS maps in Figure 4 (a-b). Because the tribological tests are run in air, a thin mixed oxide formed on the unworn background of the sample during tribotesting. Within the wear track, it appears that enhanced oxidation due to reactive broken bonds led to the formation of a mixed chromium-iron oxide during cool down.

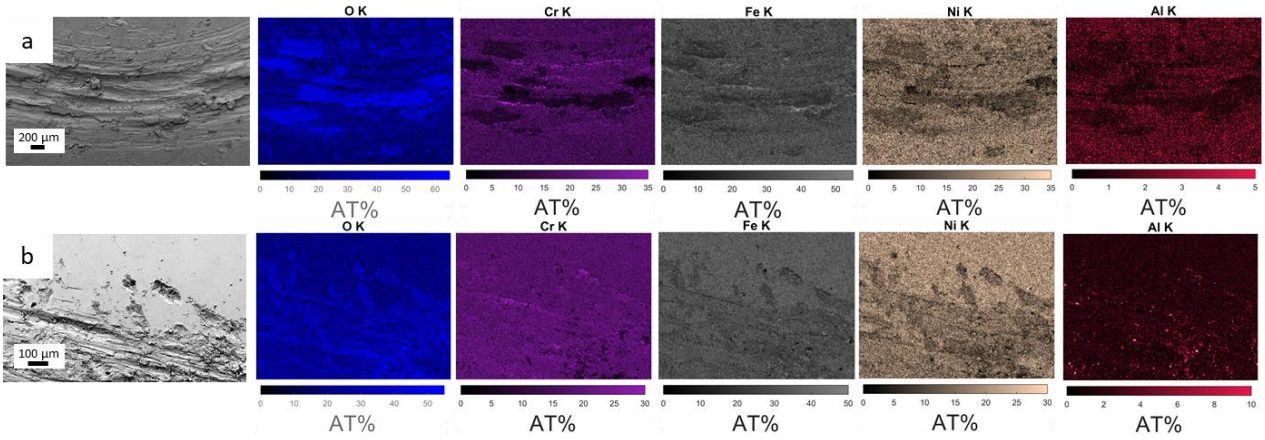

Figure 4: Plan-view SEM images and EDS maps of the wear tracks for as-received alloy 800HT after wear testing at 750 °C under (a) 1N load and (b) 5N load.

Micrographs of the wear tracks for conditioned alloy 800HT are shown in Figure 5 (a-d). At low load, the oxide layer formed during conditioning was able to withstand the contact stresses and was compacted at high temperature into a smooth glaze-oxide layer via sintering as shown on Figure 5 (b). Nanohardness measurements demonstrate that the glaze oxide is much harder than the as-received

material (14.7 ± 0.9 GPa versus 4.9 ± 0.3 GPa, respectively). However, at higher load, the oxide broke through (in 5 out of 7 tests), and wear mechanisms similar to those of as-received alloy 800HT (namely, gouging and scuffing) are present. These observations are consistent with the results of Figure 2 (b) that suggest that two distinct wear mechanisms can result, depending on whether or not a protective oxide is present and remains on the surface throughout the duration of the tribotest. Spherical particles visible on Figure 5 (b) are oxide particles that formed during cooldown of the sample and do not play a role in the tribological behavior. SEM micrographs of the wear tracks show similar wear severity between as-received samples and conditioned samples with oxide breakthrough which is consistent with their similar wear volumes.

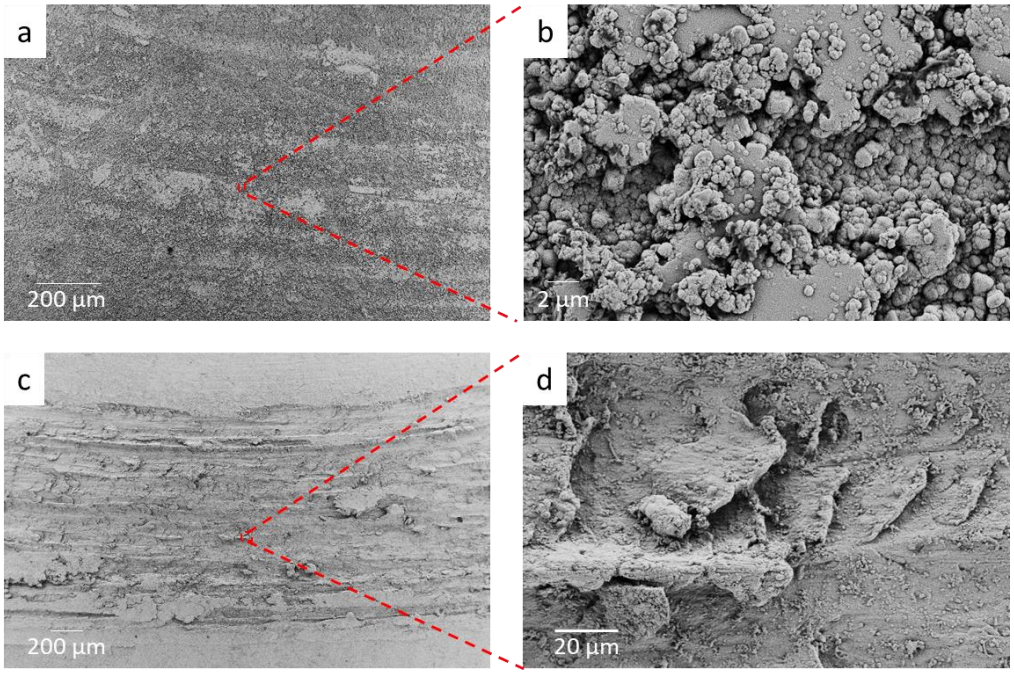

Figure 5: Morphology of the wear tracks for conditioned alloy 800HT after wear testing at 750 °C under (a, b) 1N load and (c, d) 5N load [16].

The compositions of the wear track and of the unworn surface for conditioned alloy 800HT with the two possible wear cases at high load - oxide breakthrough or glaze-oxide layer formation - are shown in the plan-view EDS maps in Figure 6. The exposure to air during tribotesting enabled the formation of a mixed and discontinuous Ni-Fe oxide on top of the pre-existing Cr oxide in the background of all samples. Figure 6 (a, c) provides evidence that the glaze-oxide layer formed consists of Ni-Fe oxide that developed on top of the pre-existing oxide.

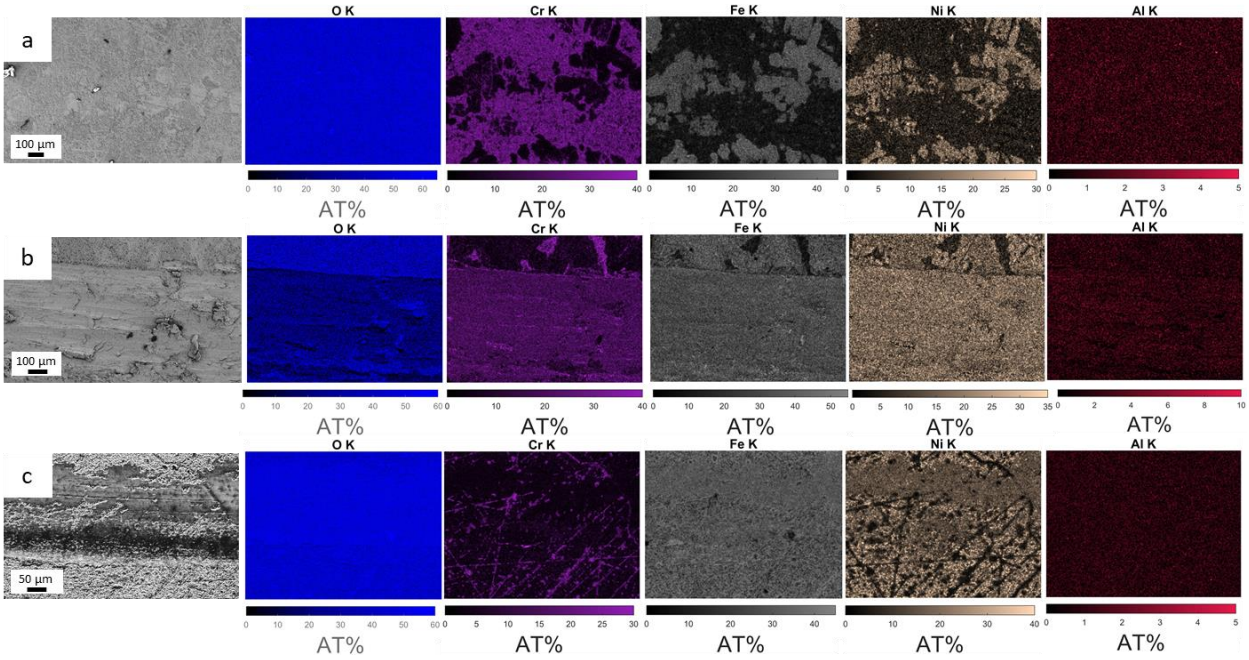

Figure 6: Plan-view SEM images and EDS maps of the wear tracks for conditioned alloy 800HT after wear testing at 750 °C under (a) 1N load, (b) 5N load, revealing oxide breakthrough, and (c) 5N load, revealing glaze-oxide-layer formation.

The results of this section have shown that a pre-existing oxide can dramatically improve the wear resistance of alloy 800HT if the applied load is below the oxide breakthrough threshold. When a glaze layer formed, both the initial friction coefficient and the wear volumes dropped significantly.

3.1.2. Kolsterised samples with and without conditioning

In an effort to enhance the wear resistance of alloy 800HT, samples were Kolsterised to increase the surface hardness via carbon solid solution strengthening [19]. In addition to Kolsterising®, some samples were also conditioned to study the effect of HTGR environment on corrosion and tribology.

3.1.2.1. Corrosion results

Figure 7 shows a cross-sectional SEM micrograph and a GDOES depth scan of Kolsterised alloy 800HT. Kolsterising® increased the carbon content up to 20 at% at the surface, which decreased down to the background level at a depth of 23 µm [Figure 7 (b)]. The stoichiometry at the surface of the sample was confirmed via XPS and is consistent with the carbon supersaturation observed in 316SS, another austenitic steel [19,20]. Additionally, neither the micrograph nor the GDOES scan indicated the presence of an oxide due to the Kolsterising® treatment.

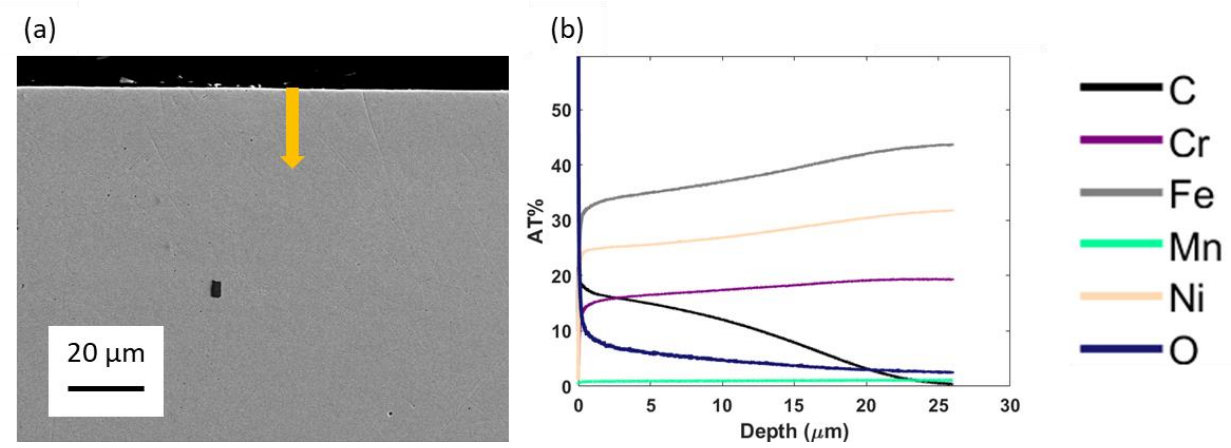

Figure 7: (a) Cross-sectional SEM image and (b) GDOES depth scan of Kolsterised alloy 800HT.

To investigate potential carbide formation, XRD was performed on the as-received and Kolsterised alloy 800HT. The XRD patterns (shown in Figure S2) indicate that no additional phases emerged after Kolsterising®, which is consistent with the absence of carbide precipitation expected with the low-temperature process. A shift in the pattern has been noted, which is due to the higher lattice parameter caused by the entrapment of carbon atoms in interstitial sites of the alloy.

Figure 8 shows a SEM cross-sectional micrograph, an EDS line scan, and a GDOES depth scan of Kolsterised alloy 800HT after conditioning. The carbon profile is not included in the EDS line scan of Figure 8 (b) due to inaccuracies inherent in measuring carbon concentration via EDS. An external Cr-Mn oxide formed on top of a thin internal Al oxide layer for a total oxide thickness of 3.98 ± 0.62 µm. As seen in the SEM image of Figure 8 (a), the external oxide layer appears to be non-uniform, and the interface between the external oxide and the internal oxide does not appear to be robust. Additionally, Figure 8 (c) indicates that the carbon content at the surface decreased down to 5 at%. The increased Ti content visible at 20 µm from the surface on Figure 8 (b) is due to a pre-existing Ti carbide [21]. This precipitate is sub-surface and does not impact the wear behavior.

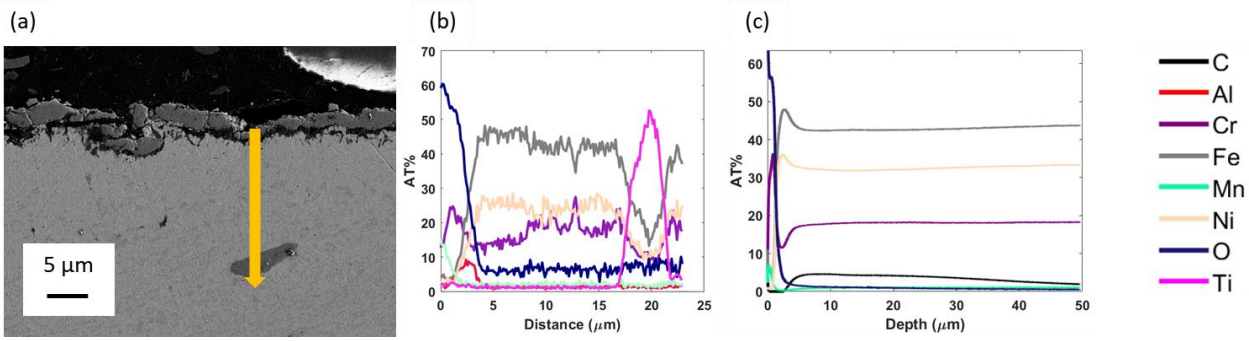

Figure 8: (a) Cross-sectional SEM image, (b) EDS line scan, and (c) GDOES depth scan of alloy 800HT after Kolsterising® followed by conditioning.

3.1.2.2. Tribological results

The wear volumes for as-received and Kolsterised alloy 800HT tested at 650 °C and 750 °C are shown in Figure 9 (a, b) as a function of load and initial friction coefficient, respectively. As described in Section

3.1.1.2., the testing temperature does not have a measurable impact on the tribological behavior over this temperature range. The wear volumes and associated uncertainties of Kolsterised samples are much lower than those of as-received alloy 800HT at every load. In contrast with the conditioned samples, no threshold load is observed for transitioning between wear mechanisms for the Kolsterised samples. Figure 9 (b) supports this observation, with all Kolsterised samples exhibiting similar low initial friction coefficients (~0.5) independent of the load and wear volume.

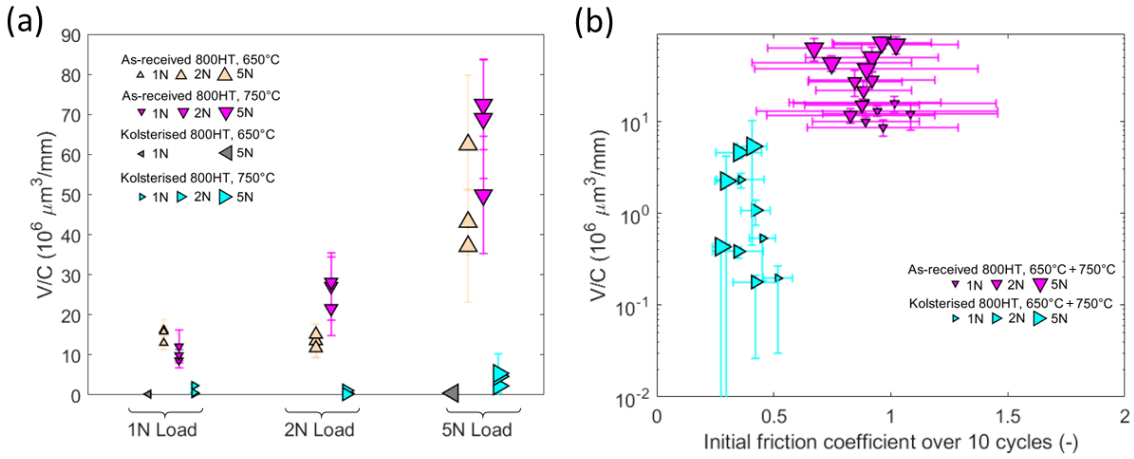

Figure 9: Wear volumes as a function of (a) load and (b) initial friction coefficient for as-received alloy 800HT and Kolsterised alloy 800HT. The temperature during wear testing is stated in the legend labels. A 3D rotational version of these data is available as an interactive plot.

Figure 10 shows the wear volumes for conditioned alloy 800HT and alloy 800HT after Kolsterising® followed by conditioning. All samples that were Kolsterised and then conditioned have the same initial friction coefficient, independent of load and measured wear volume, which suggests a consistent wear mechanism for this type of sample. The initial coefficient of friction is higher for samples after Kolsterising® followed by conditioning compared to the coefficient of friction for conditioned samples that developed a glaze-oxide layer, and it is close to the coefficient of friction of the samples which experienced oxide breakthrough. Comparing the two cases of conditioned samples, wear was measurable even at low load for alloy 800HT after Kolsterising® followed by conditioning, suggesting that the negligible-wear threshold for that sample is less than 1 N. In addition, for the same samples, the wear volumes from individual tests are more tightly grouped, and the wear volume uncertainties are smaller, indicating more consistent wear behavior at a given load.

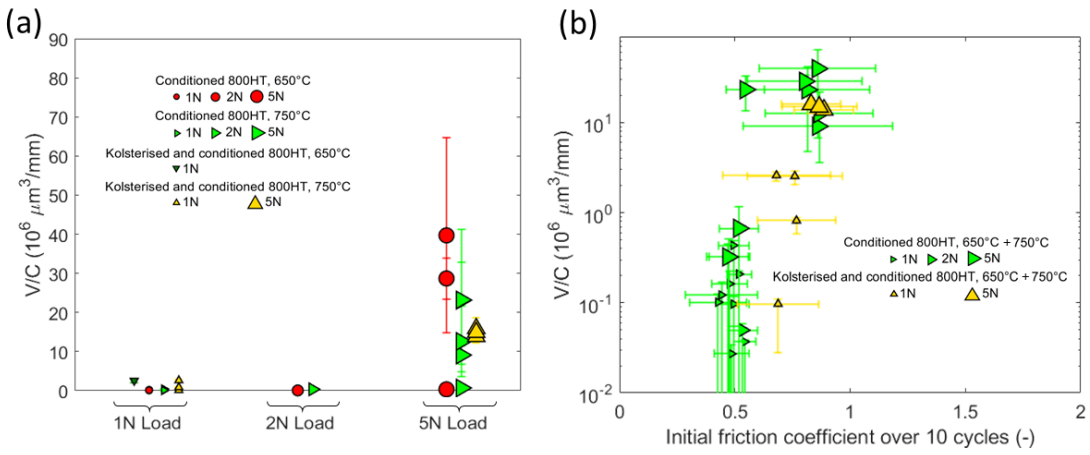

Figure 10: Wear volumes as a function of (a) load and (b) initial friction coefficient for conditioned alloy 800HT and alloy 800HT after Kolsterising® followed by conditioning. The temperature during wear testing is stated in the legend labels. A 3D rotational version of these data is available as an interactive plot.

SEM micrographs of the wear tracks for Kolsterised alloy 800HT are presented on Figure 11 (a-d). At low load, a glaze oxide appears to have formed on the surface and protected the surface as shown in Figure 11 (b) despite no pre-existing oxide being present initially. It is also important to note the presence of debris in the wear track which provides evidence that surface experienced wear during the test. Figure 11 (d) indicates that oxide wear occurred during the tribotests at higher load.

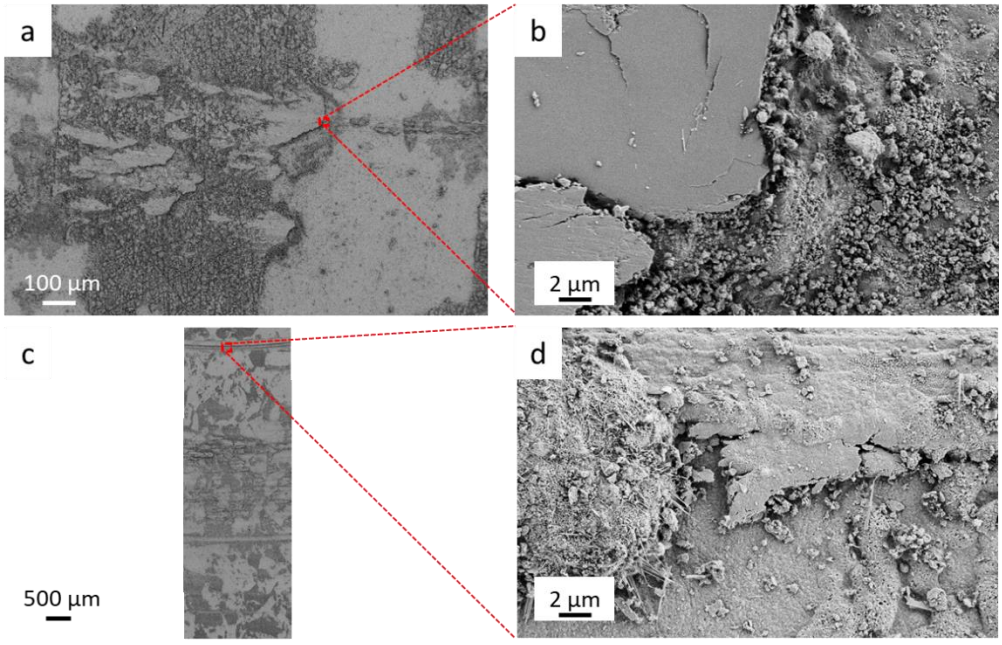

Figure 11: Morphology of the wear tracks for Kolsterised alloy 800HT after wear testing at 750 °C under (a, b) 1N load and (c, d) 5N load.

Plan-view EDS composition maps of the wear tracks for Kolsterised alloy 800HT are presented in Figure 12 (a-b). Patches of iron oxide formed on top of a mixed Cr-Mn oxide during the tribotests and led to

glaze-oxide-layer formation at low load as shown in Figure 12 (a). At high load, the oxide was continuously worn, and Figure 12 (b) shows a Cr-Mn oxide was present at the end of the tribotest.

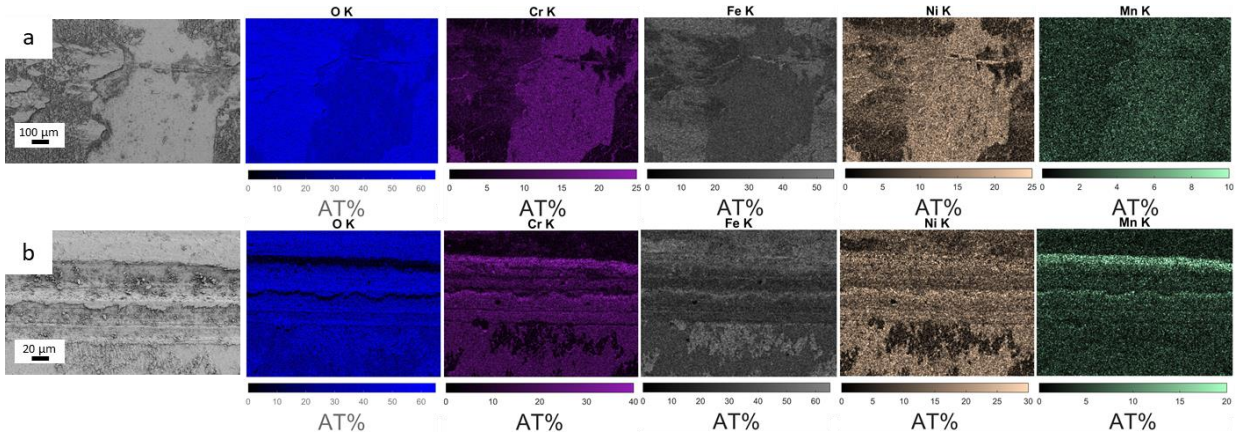

Figure 12: Plan-view SEM images and EDS maps of the wear tracks for Kolsterised alloy 800HT after wear testing at 750 °C under (a) 1N load and (b) 5N load.

SEM micrographs of the wear tracks for alloy 800HT after Kolsterising® followed by conditioning are presented on Figure 13 (a-d). At both loads, oxide breakthrough and scuffing appear to be the principal wear mechanisms, and wear debris are visible. Wear tracks for 5N tribotests are wider than for 1N tribotests, which is consistent with the wear volume increase with load. Additionally, the absence of a glaze-oxide layer indicates that wear was more severe compared to that of conditioned samples, which is consistent with the profilometry results [shown in Figure S3 (c-d) and Figure S4 (c-d), respectively]. However, Figure 13 (c, d) shows that Kolsterising® followed by conditioning slightly mitigated the wear at high load, even with evidence of oxide breakthrough followed by metal-on-metal scuffing.

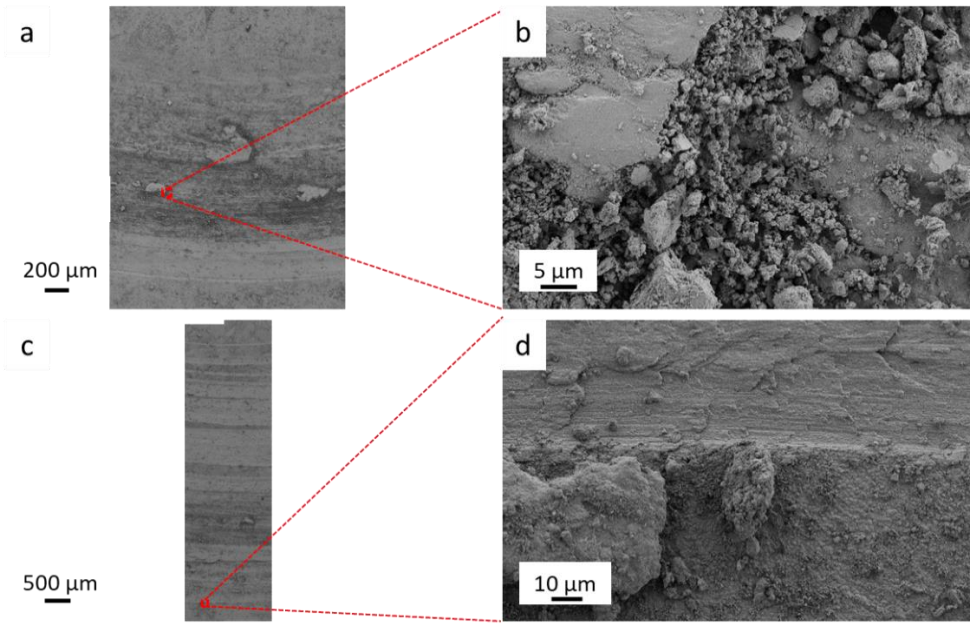

Figure 13: Morphology of the wear tracks for alloy 800HT after Kolsterising® followed by conditioning, after wearing testing at 750 °C under (a, b) 1N load and (c, d) 5N load.

Plan-view EDS composition maps of the wear tracks for alloy 800HT after Kolsterising® followed by conditioning are presented in Figure 14 (a-b). The Cr-Mn oxide formed during conditioning is still present in the background of the samples. The bulk-like composition of the wear tracks indicates that the oxide was broken through at both loads, which is consistent with the previous observations.

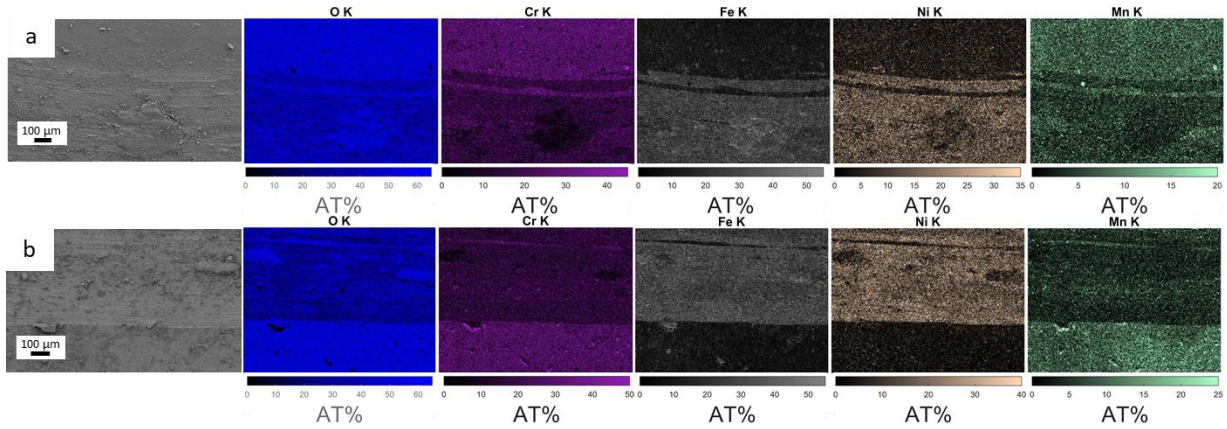

Figure 14: Plan-view SEM images and EDS maps of the wear tracks for alloy 800HT after Kolsterising® followed by conditioning, after wear testing at 750 °C under (a) 1N load and (b) 5N load.

3.2. Alloy 617

3.2.1. As-received and conditioned samples

This section provides information on the corrosion of alloy 617 in a HTGR-like environment and the impact of corrosion on high-temperature tribological behavior.

3.2.1.1. Corrosion results

Figure 15 shows the cross-sectional SEM micrograph and EDS line scan for conditioned alloy 617. The cross-sectional SEM micrograph and EDS line scan of as-received alloy 617 is shown in Figure S5 of the supplemental material as a baseline reference. The compositional profile of conditioned alloy 617 indicates the formation of an external chromium oxide with a deeper internal aluminum oxide along grain boundaries. Figure 15 (a) shows enhanced surface oxidation occurred at grain boundaries (highlighted in red), leading to a non-uniform oxide growth across the surface of conditioned alloy 617, as observed in [22]. The thickness of the oxide on the grain boundaries is 3.50 ± 0.17 µm, and the thickness of the oxide on the grains is 1.00 ± 0.20 µm. The composition of the external grain boundary oxide is comparable to that on the grains. Despite the lack of uniformity, the interface between the external oxide and the alloy appears to be continuous and robust.

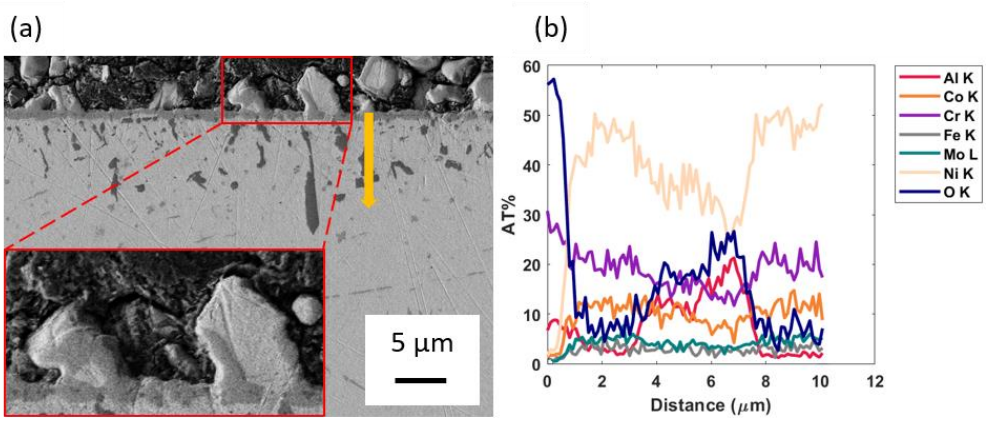

Figure 15: (a) Cross-sectional SEM image and (b) EDS line scan of conditioned alloy 617.

3.2.1.2. Tribological test results

The wear volumes for as-received and conditioned alloy 617 are presented in Figure 16 (a, b) as a function of load and initial friction coefficient, respectively. Similar to alloy 800HT, the testing temperature does not have a measurable impact on the tribological behavior over this temperature range. As found by Rahman et al. in [23], in the as-received case, the wear volume and associated uncertainty increases with increasing load and becomes measurable at high load. Yet, all but one of the conditioned samples exhibited wear below the detection threshold of the measurement technique. It appears that alloy 617 is wear resistant at low and medium loads in the as-received state, and that conditioning improves the wear resistance at higher load. At 5N load, the oxide layer remained protective in six out of the seven samples tested. The results of Figure 16 (b) do not display the strong correlation between initial friction coefficient and wear volume that was revealed for alloy 800HT. The data are clustered based on initial friction coefficient, with as-received alloy 617 exhibiting distinctly higher initial friction than conditioned 617; however, they are not distinguished in terms of wear volume. Subsequent characterization results will elucidate the different wear mechanisms.

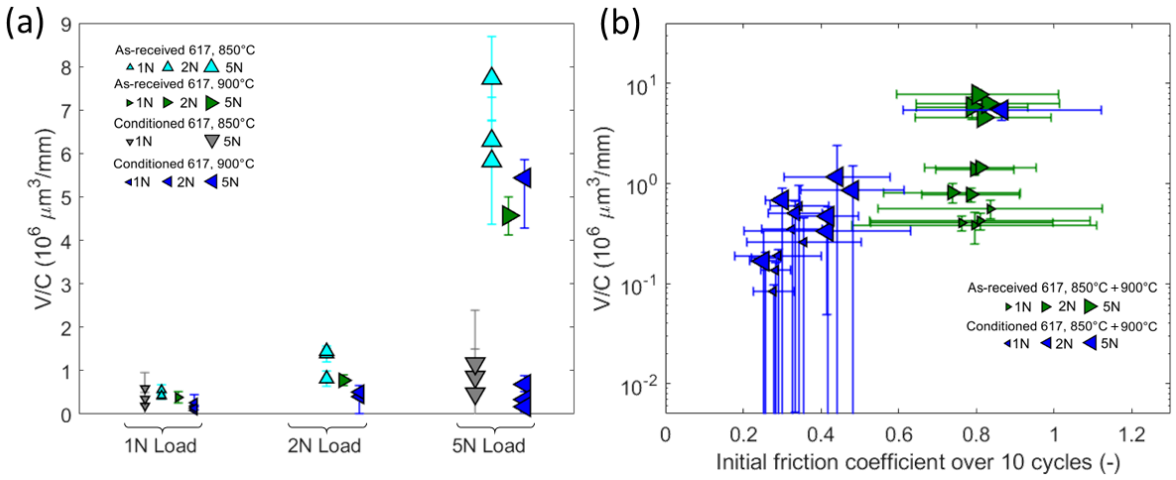

Figure 16: Wear volumes as a function of (a) load and (b) initial friction coefficient for as-received alloy 617 and conditioned alloy 617. The temperature during wear testing is stated in the legend labels. A 3D rotational version of these data is available as an interactive plot.

SEM micrographs of the wear tracks for as-received alloy 617 are shown in Figure 17 (a-d). Similar to alloy 800HT, scuffing and gouging dominated the wear at both loads, and no evidence of oxide compaction is observed. The wear track appears narrower for the 1N-load test [Figure 17 (a)] than for the 5N-load test [Figure 17 (c)]. Less debris is visible outside of the wear track, and the overall wear is less severe compared to that of alloy 800HT.

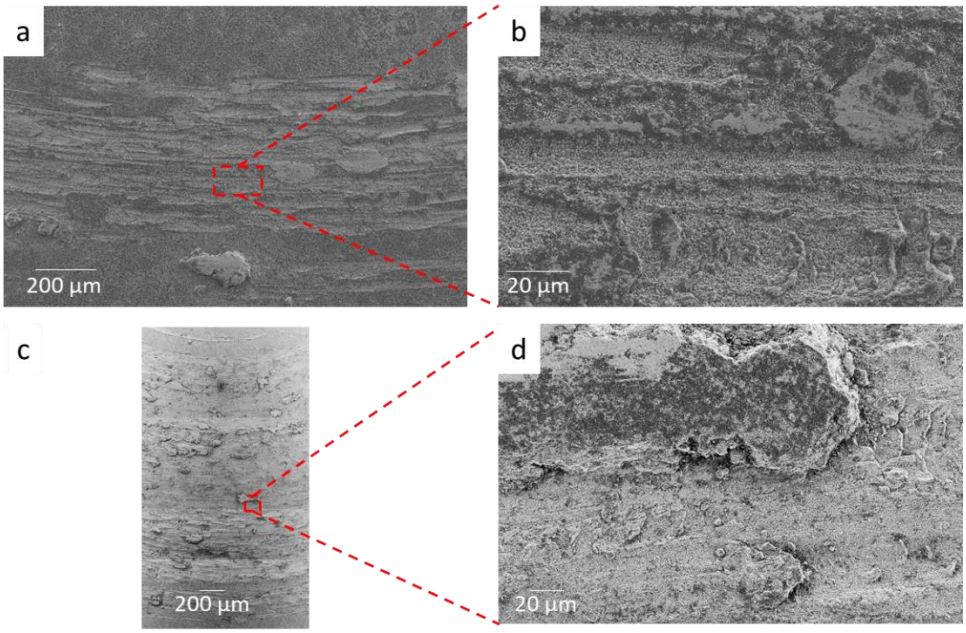

Figure 17: Morphology of the wear tracks for as-received alloy 617 after wear testing at 900 °C under (a, b) 1N load and (c, d) 5N load [16].

Plan-view EDS composition maps of the wear tracks for as-received alloy 617 are shown in Figure 18 (a-b). A thin Al-enriched oxide formed on the background of the sample during tribotesting due to the high-temperature exposure to air. Reactive broken bonds created during wear testing in the wear track increased the oxidation rate, and a chromium oxide formed on the worn surface during the cooldown period.

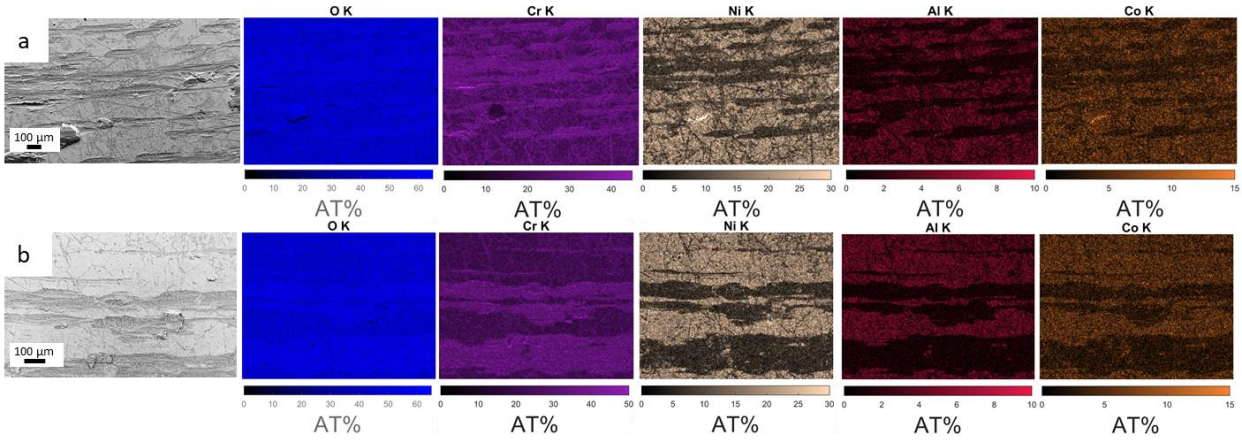

Figure 18: Plan-view SEM images and EDS maps of the wear tracks for as-received alloy 617 after wear testing at 900 °C under (a) 1N load and (b) 5N load.

SEM micrographs of the wear tracks for conditioned alloy 617 are shown in Figure 19 (a-d). At both loads, the oxide layer formed during conditioning was able to withstand the contact stresses. In particular, the thicker oxide that developed at the grain boundaries supported the load and was compacted into a smooth glaze oxide via sintering as shown on Figure 19 (b, d). This cross-link structure of oxide on the grain boundaries has also been observed by He et al. [24] for chromium oxide coatings on Inconel™ 718 after annealing at 1000 °C for 2 h. Similar to alloy 800HT, nanohardness measurements indicate that the glaze oxide is much harder than the as-received material (13 ± 2 GPa and 6.7 ± 0.5 GPa, respectively). This sharp increase in hardness was also reported by Salari et al. [25]. These observations are consistent with the results of Figure 16 (b) that suggest that a distinct wear mechanism is at play when the oxide layer remains intact throughout the duration of the tribotest. The overall depth of the wear track and severity of the wear at low load appear similar for as-received and conditioned samples, which is consistent with the wear volume results shown in Figure 16. The difference in wear severity at high load between as-received and glaze-oxide-protected samples presented in Figure S6 (a-d) is mild, and is consistent with the small difference in wear volumes between the two cases at high load (~$6x10^6$ μm^3/mm for alloy 617 as opposed to ~$60x10^6$ μm^3/mm for alloy 800HT).

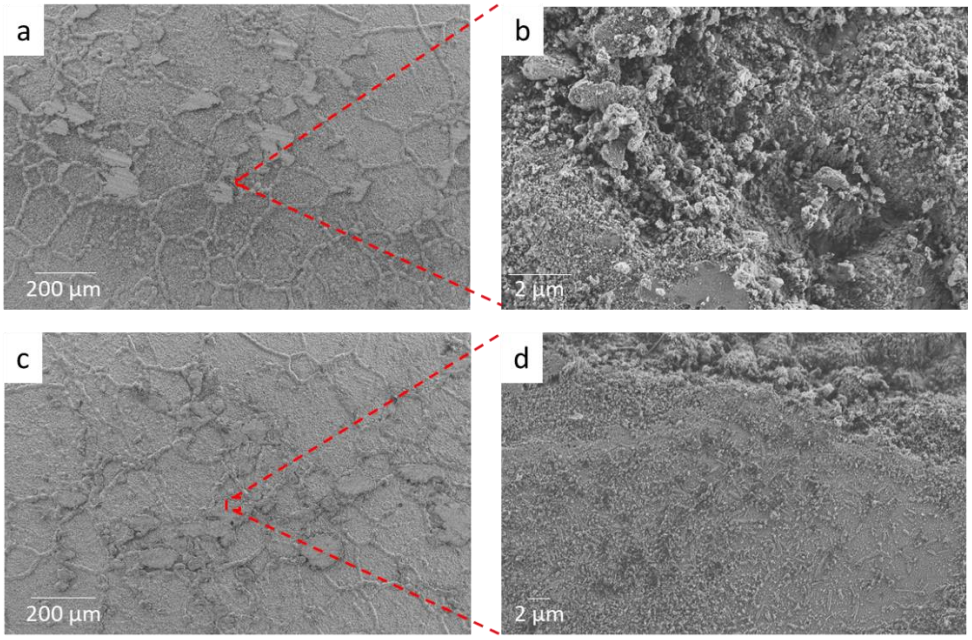

Figure 19: Morphology of the wear tracks for conditioned alloy 617 after wear testing at 900 °C under (a, b) 1N load and (c, d) 5N load [16].

Figure 20 shows plan-view EDS maps of the wear tracks for conditioned alloy 617. The chromium oxide formed during conditioning is present in the background. The glaze-oxide layer is discontinuous and is present in patches along the wear track. Figure 20 shows that the 'glaze' oxide layer has a composition with approximately the same metallic proportions as those of the bulk material. This composition has been observed for alloy 617 [26] since, at high temperature, the glaze oxide consists of spinel oxide compound, $NiCr_2O_4$. Additionally, the high-temperature exposure to air slightly increased the Al and Ti content of the oxide on the grain boundaries.

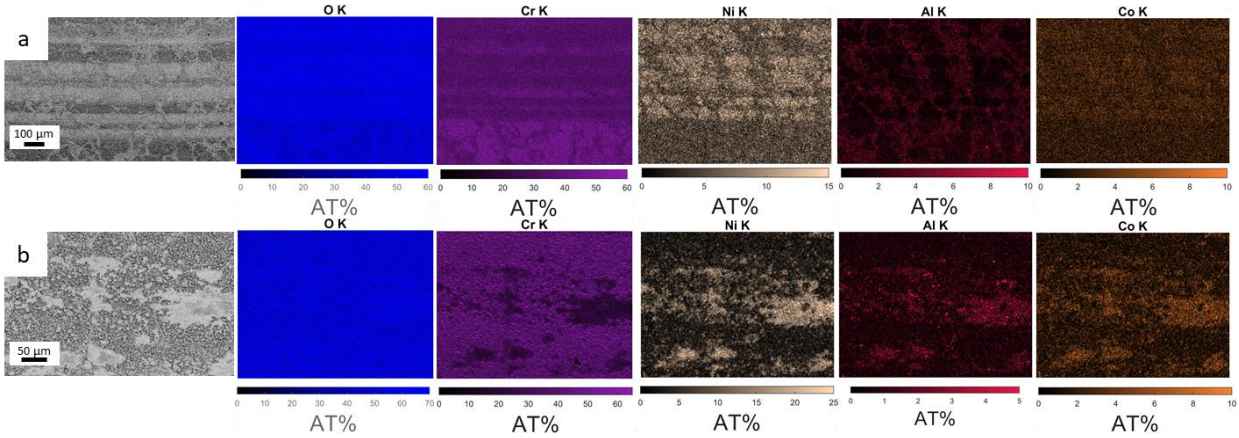

Figure 20: Plan-view SEM images and EDS maps of the wear tracks for conditioned alloy 617 after wear testing at 900 °C under (a) 1N load and (b) 5N load.

3.2.2. Kolsterised samples

Alloy 617 was also Kolsterised with the goal of increasing wear resistance, however, the effect of conditioning was not explored for this alloy.

3.2.2.1. Corrosion results

Figure 21 shows a cross-sectional SEM micrograph and a GDOES depth profile of Kolsterised alloy 617. The carbon content increases to 10% at the surface and decreases down to the baseline level at about 9 µm below the surface, as shown on Figure 21 (b). The stoichiometry at the surface is consistent with the level achieved with a similar low-temperature carbon diffusion process on other Ni-based superalloys [27]. Additionally, neither the SEM micrograph nor the GDOES profiles indicate the presence of an oxide after Kolsterising®.

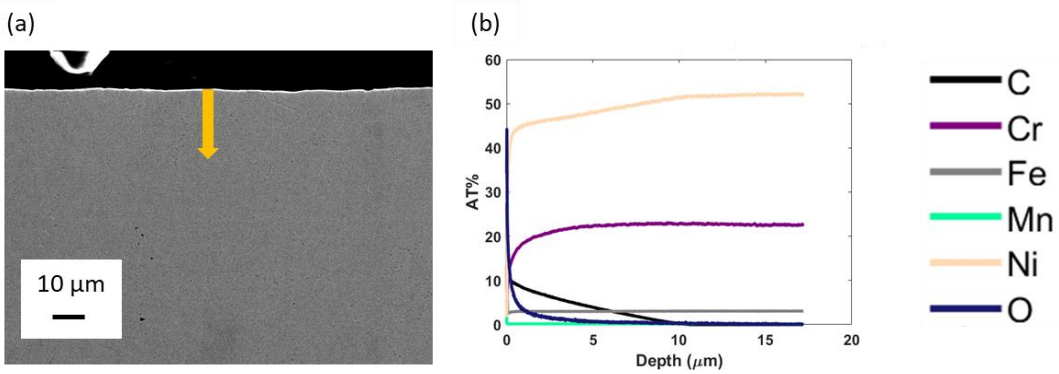

Figure 21: (a) Cross-sectional SEM image and (b) GDOES depth scan of Kolsterised alloy 617.

Similar to alloy 800HT, the XRD patterns of as-received and Kolsterised alloy 617 (shown in Figure S7) indicate that no additional phase emerged after Kolsterising®. However, the supersaturation of the alloy lattice by carbon induced a slight shift in the peaks due to the increase in lattice parameter.

3.2.2.2. Tribological test results

The wear volumes of the tribotests for as-received and Kolsterised alloy 617 are shown in Figure 22 (a, b) as a function of load and initial friction coefficient, respectively. The wear volumes and associated uncertainties of Kolsterised samples are lower (especially at high load) than those of as-received alloy 617. Figure 22 (b) indicates that Kolsterised samples exhibit initial friction coefficients similar to those of as-received alloy 617 independent of the load and wear volume. This suggests that the two conditions result in the same wear mechanism: the difference in wear volume is likely due to a harder surface rather than a different wear mechanism.

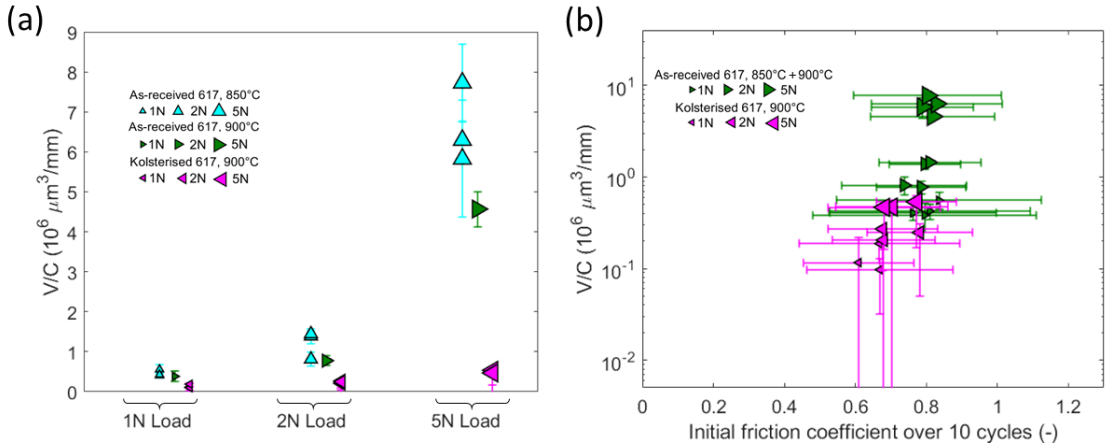

Figure 22: Wear volumes as a function of (a) load and (b) initial friction coefficient for as-received alloy 617 and Kolsterised alloy 617. The temperature during wear testing is stated in the legend labels. A 3D rotational version of these data is available as an interactive plot.

SEM micrographs of the wear tracks for Kolsterised alloy 617 are shown in Figure 23 (a-d). At both loads, mild scuffing and material removal occurred first, followed by debris build-up and compaction. The compacted debris then become the load-bearing areas of the wear tracks. For both loads, the wear tracks of Kolsterised samples [Figure S8] appear narrower and shallower than those of as-received samples shown in Figure S6 (a, b). These results are consistent with the conclusions from the wear volume plots on Figure 22 (a).

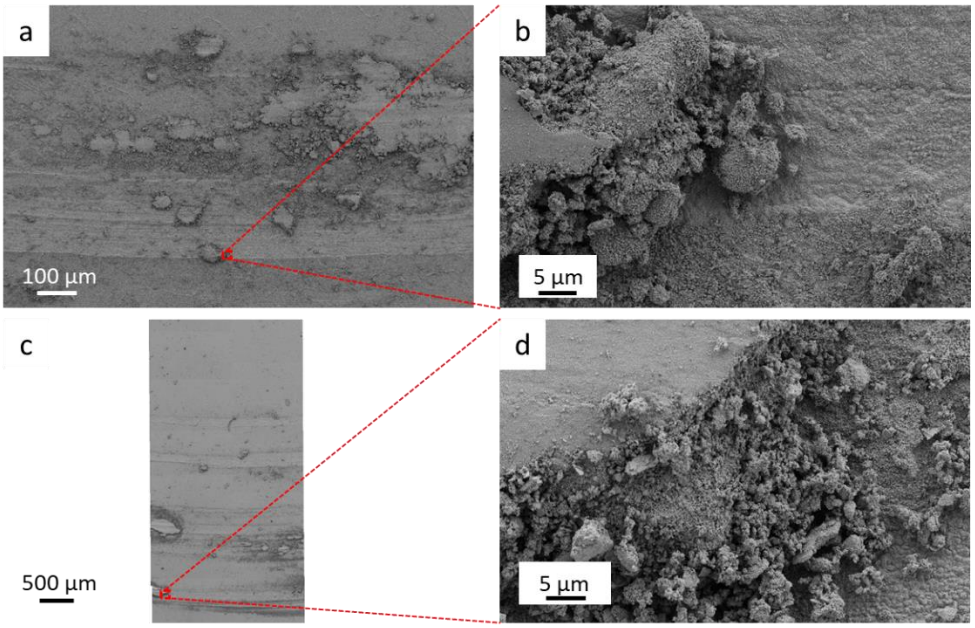

Figure 23: Morphology of the wear tracks for Kolsterised alloy 617 after wear testing at 900 °C under (a, b) 1N load and (c, d) 5N load.

Plan-view EDS maps of the wear tracks for Kolsterised alloy 617 are shown in Figure 24 (a-b). The load-bearing areas described previously exhibit a bulk-like composition with a mild degree of oxidation. However, the oxidation rate of Kolsterised alloy 617 seems to be too low to trigger the formation of a glaze-oxide layer. The background of the sample outside of the wear track developed a typical external chromium oxide on top of an internal aluminum oxide.

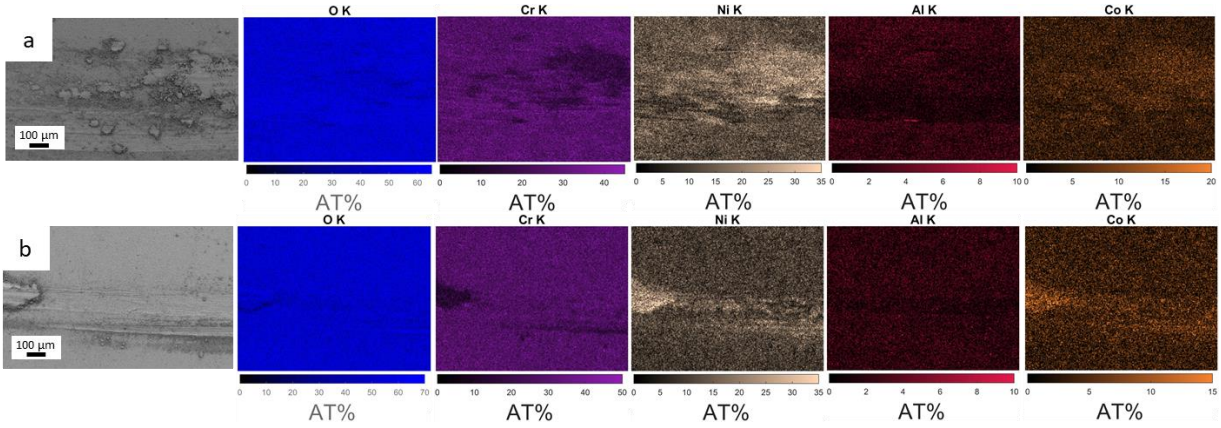

Figure 24: Plan-view SEM images and EDS maps of the wear tracks for Kolsterised alloy 617 after wear testing at 900 °C under (a) 1N load and (b) 5N load.

4. DISCUSSION

4.1. Literature

The tribological behavior of superalloys, both Ni-based and austenitic steels, has been the subject of several recent publications because of their relevance to extreme environments like that of HTGRs [16,18,22,23,25,28,29]. Rahman et al. [28] reported the chemistry of the oxides formed on alloy 617 and 800HT after testing at high temperatures in air and He environments. They observed poor adherence and limited ductility of the oxide layer on alloy 800HT, which led to failure and increased wear at elevated temperatures. Following tribotesting, elemental analysis revealed the presence of Cr_2O_3, $NiCr_2O_4$, TiO_2 and $MnTiO_3$ oxides on the surface of alloy 617, and Fe-Cr-Al oxide on the surface of alloy 800HT [22,23,28]. In our present study, cross-sectional elemental analysis revealed the presence of an external Cr-rich oxide and an internal grain boundary Al oxide for alloy 800HT, and an external Ni-Cr oxide combined with an internal grain boundary Al oxide for alloy 617.

Rahman et al. [28] also reported on the in-situ tribological behavior of alloys 800HT and 617 at elevated temperatures. For samples tested in air, the steady-state coefficients of friction of both alloys dropped at elevated temperatures – for alloy 617, the friction coefficient dropped from 1.1 at 23 °C to 0.47 at 800 °C; for alloy 800HT, the coefficient dropped from 1.28 at 23 °C to 0.66 at 750 °C. A similar decreasing trend with increasing temperature was reported for alloy 617 by Ahmadi et al. [29]. The steady-state coefficients of friction were higher in He environment for both alloys; namely, 1.48 for Inconel 617 at 800 °C, and 1.66 for alloy 800HT at 750 °C [28]. The difference between air and He environments was attributed to the formation of a glaze-oxide layer for samples tested in air. This observation agrees with the measurements of our present study: conditioned samples where a ‘glaze’ layer formed exhibited lower initial friction coefficients than those with oxide breakthrough. Additionally, no specific trends for variations in steady-state friction coefficients as a function of applied load for alloys 617 and 800HT have been reported in the literature [18,23]. For alloy 617 tribotested in a high-temperature air environment, Rahman et al. [23] concluded that, unlike the applied load, the oxidation and tribochemistry at the contact have a dominant effect on the friction coefficient. Our present study has shown similar results, but also provides evidence that the applied load can significantly change the chemistry of the surface and thus the friction coefficient.

Rahman et al. [18,23] reported an increasing wear rate with increasing applied load for both alloys, in agreement with results shown in this present study. They also observed an increase in wear rate with increased temperature (room temperature, 500°C and 750°C for alloy 800HT; room temperature, 500°C and 950°C for alloy 617) which was not observed in the present study due to the temperature ranges investigated (650°C and 750°C for alloy 800HT; 850°C and 900°C for alloy 617). Rahman et al. reported that the 'glaze' oxide layer becomes unstable under high contact pressure and can fail to protect the surface from wear. Our observations show that high loads are responsible for preventing 'glaze' oxide formation even with a lower contact pressure than that of low-load tests in which 'glaze' oxide formation occured. In agreement with the present study, a decrease in wear resistance of alloy 800HT compared to that of alloy 617 was observed by Rahman et al. [28]. For alloy 617, Salari et al. [25] reported that the hardness of the oxide layer is significantly higher (6.5 times at room temperature and 3.15 times at 400 °C) compared to that of the bulk. In our study, the hardness of the oxide increased by a factor of 2 over that of as-received alloy 617.

4.2. Wear mechanisms

For both alloys 800HT and 617, the wear volumes and the initial friction coefficients provide information on both the resistance to wear volume loss and the initial state of the surface, respectively. Since friction and wear are strongly coupled dynamic processes [30], the relationship between friction coefficients and wear volumes has been studied and put into perspective relative to the observed wear mechanisms. The initial friction coefficient correlates with the severity of wear immediately upon contact and provides insight into the wear mechanism. The wear volume reflects the extent to which the surface was damaged during the process of reaching steady state.

Eyre et al. [31] described several wear mechanisms including abrasive, fretting, and corrosive wear that tend to be mutually exclusive. Yet, the present observations are more complex, with a combination of all three mechanisms potentially happening at the same time in HTGR environments. Herein we base our descriptions of the wear mechanisms on the chemistry and topography of the worn surfaces. The wear mechanisms can be identified by examining the SEM-EDS maps, ranging in wear severity from high to low as follows: (i) base-metal wear characterized by gouging, scuffing, and debris formation followed by debris redeposition within the wear track; (ii) oxide breakthrough followed by wear of the base alloy; (iii) oxide wear without breakthrough; (iv) oxide compaction leading to the formation of a protective glaze oxide, with no wear of the underlying base metal. It is generally agreed that scuffing/gouging is a running-in problem that leads to the greatest degree of surface topographical changes [31]. Thus, it is consistent with the consensus that we find that the scuffing/gouging mechanism leads to the most severe wear.

4.3. Effect of conditioning

When the surfaces of conditioned alloys remained undamaged due to the formation of a protective glaze-oxide layer, the initial friction coefficients were half, on average, of those of both as-received samples and conditioned samples that experienced oxide breakthrough. For example, for alloy 800HT, the initial coefficient of friction for conditioned alloy 800HT that did not experience oxide breakthrough was 0.494 +/- 0.044, whereas the initial as-received coefficient of friction was 0.904 +/- 0.126, and the initial coefficient of friction for conditioned 800HT that experienced oxide breakthrough was 0.820 +/-

0.122. Similarly, for alloy 617, the initial coefficient of friction for conditioned alloy 617 that did not experience oxide breakthrough was 0.341 +/- 0.075, whereas the initial as-received coefficient of friction was 0.804 +/- 0.077 and the initial coefficient of friction for conditioned 617 that experienced oxide breakthrough was 0.867 +/- 0.255. Thus, the differences in the initial coefficient are due to the degree to which the surface oxide can support the load without being broken through. The SEM-EDS maps confirm the oxide-breakthrough mechanism suggested by the trends in initial friction coefficient. Wear volumes within the same order of magnitude for as-received samples and conditioned samples with oxide breakthrough demonstrate that the hardness of the base metal strongly influences the resistance to volume loss either when no protective oxide is present or when the surface oxide that is present is not of sufficient mechanical integrity. For example, at 5 N applied load, the wear volume for as-received 800HT was 55.65 +/- 15.45 x 10^6 μm^3/mm, and the wear volume for as-received 617 was 6.10 +/- 1.39 x 10^6 μm^3/mm. These values are within the same order of magnitude as those found by Rahman et al. when assuming a wear track diameter of 17.5mm: ~11 x 10^6 μm^3/mm and ~8 x 10^6 μm^3/mm for alloy 800HT at 750°C under a 5N load with a sliding velocity of 0.04 m/s and alloy 617 at 950°C under a 5N load with a sliding velocity of 0.1 m/s, respectively [18,23]. For conditioned alloys that experienced oxide breakthrough, also at 5 N load, the wear volume for conditioned alloy 800HT was 22.63 +/- 14.00 x 10^6 μm^3/mm, and the wear volume for conditioned alloy 617 was 5.44 +/- 0.87 x 10^6 μm^3/mm. Similar trends for the wear volumes and friction coefficients were reported by So et al. [32] for steels; the wear rate and friction coefficient of oxidational wear were lower by several orders of magnitude and a factor of 2, respectively, than those of abrasive wear. The yield strength of 617 at 850-900 °C is higher than that of 800HT at 650-750 °C (256 – 169 MPa versus 120-123 MPa, respectively), which explains the relatively higher wear volumes of 800HT compared to 617 when the base metal is worn (discussed in more detail in [16]). When the oxide is protective, and glaze-oxide-layer formation occurs, wear volumes are negligible.

4.4. Effect of Kolsterising®

Initial friction coefficients for Kolsterised alloy 800HT were half, on average, of those of as-received alloy 800HT despite the surfaces of both samples being unoxidized initially - $\mu_{initial}$ = 0.385 +/- 0.078 for Kolsterised 800HT; $\mu_{initial}$ = 0.904 +/- 0.126 for as-received 800HT. This difference is due to the rapid oxide formation on the Kolsterised alloy 800HT surface during the temperature ramp of the tribometer. Figure 25 shows GDOES depth profiles of the alloy 800HT background surfaces after tribotesting. According to this, significant surface oxidation occurred on Kolsterised 800HT down to a depth of ~12 µm. Similar initial friction coefficients for all Kolsterised samples indicate that oxide wear was the dominant mechanism at the start of the tribotests for every load. At low load, the oxidation rate enhanced by the Kolsterising process led to the formation of a glaze-oxide layer, with wear volumes similar to those of conditioned samples with a glaze oxide. At high load, the oxide was worn but was still able to support the load and prevent wear of the underlying base metal which is consistent with the strong influence of substrate hardness on the resistance to volume loss described above. The wear volumes of the Kolsterised samples were between those of the conditioned samples that experienced glaze-oxide-layer formation and conditioned samples that experienced oxide breakthrough. For example, at 5 N load, wear volume was 3.15 +/- 2.64 x 10^6 μm^3/mm for Kolsterised alloy 800HT.

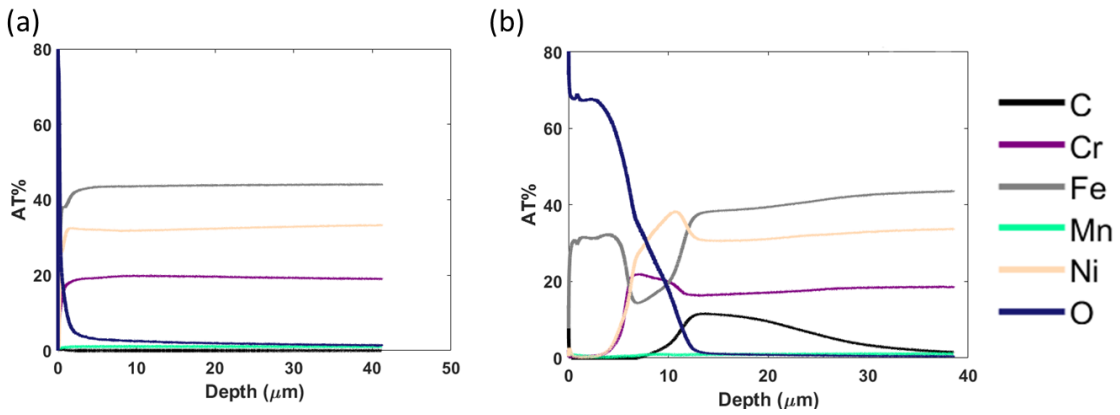

Figure 25: GDOES depth scans after wear testing at 750 °C for both (a) as-received alloy 800HT and (b) Kolsterised alloy 800HT.

Unlike alloy 800HT, initial friction coefficients for Kolsterised alloy 617 have comparable values (0.693 ± 0.077) to those of as-received alloy 617, which is consistent with scuffing of the base metal observed in the SEM-EDS maps for both conditions. Figure 26 shows GDOES depth scans for as-received and Kolsterised alloy 617 after tribotesting. The profiles of Figure 26 confirm that the oxidation rate was only slightly enhanced by the Kolsterising® process; therefore, any oxide formed during temperature ramp-up of the tribometer was insufficient to protect the base alloy from experiencing wear. The wear volumes for Kolsterised samples compared to as-received samples are significantly lower, likely due to the increased hardness of the surface caused by the increased carbon content. For example, at 5 N load, wear volume was 0.49 +/- 0.18 x 10^6 μm^3/mm for Kolsterised alloy 617.

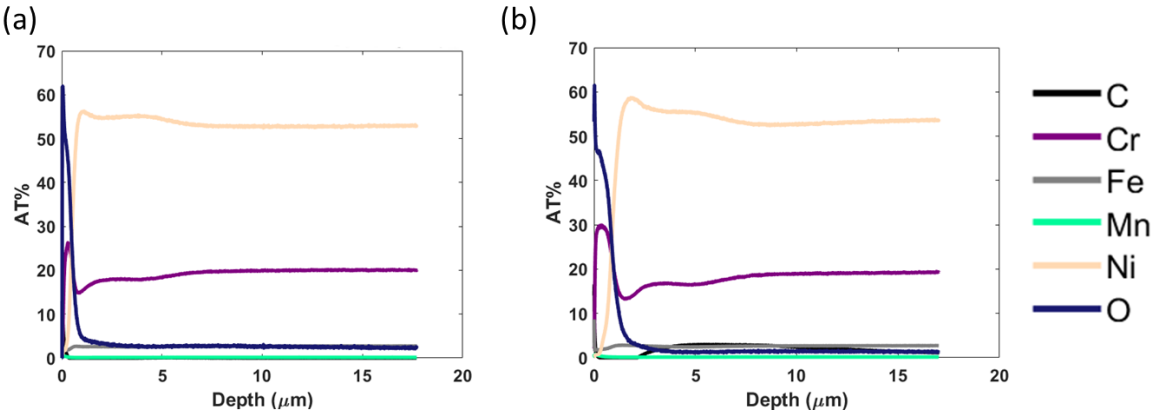

Figure 26: GDOES depth scans after wear testing at 900 °C for both (a) as-received alloy 617 and (b) Kolsterised alloy 617.

4.5. Combined effect of Kolsterising® and conditioning

At every load tested, alloy 800HT after Kolsterising® followed by conditioning exhibited initial friction coefficients similar to those of conditioned samples that experienced oxide breakthrough, which is consistent with scuffing and debris being present for both conditions. At 5 N load, $\mu_{initial}$ was 0.861 +/- 0.086 for 800HT after Kolsterising® followed by conditioning, and $\mu_{initial}$ was 0.820 +/- 0.122 for conditioned 800HT with oxide breakthrough. Surface chemistries were slightly different between the

two types of samples due to the increased Mn content in the oxide induced by Kolsterising®, but friction coefficients were similar because of similar wear mechanisms. The lower wear volumes of samples after Kolsterising® followed by conditioning compared to those of conditioned samples with oxide breakthrough are due to the enhanced hardness of the substrate from the increased carbon concentration. For example, at 5 N load, wear volume was 14.87 +/- 1.57 x 10^6 μm^3/mm for alloy 800HT after Kolsterising® followed by conditioning, and wear volume was 22.63 +/- 14.00 x 10^6 μm^3/mm for conditioned 800HT with oxide breakthrough. The lack of robustness of the interface between the internal and external oxide formed on the Kolsterised samples prevented the formation of a protective glaze-oxide layer, and a mild degree of base metal wear still occurred.

4.6. Primary factors governing wear resistance

The plots of wear volume as a function of initial friction coefficient are useful tools for determining the wear mechanism taking place for a given initial surface condition. Similar graphical methods of identification have been studied previously [33,34] where testing/operational parameters were used to predict wear mechanisms. Such maps are able to provide a global picture of how materials in relative motion behave when different sliding conditions are encountered. The maps depict wear-mechanism regime as a function of sliding condition and can be used to predict wear rates [33,34]. However, several results reported in the present study demonstrate that initially similar conditions can yield dramatically different wear results due to stochastic effects (e.g. inconsistent glaze-oxide formation on conditioned 800HT at high load). Therefore, the history of the friction coefficient throughout the wear process, particularly the friction coefficient at the beginning of the test, provides valuable insight into the wear mechanism both during early-stage wear and steady-state.

It is important to note that, in addition to initial coefficients of friction, steady-state coefficients of friction were also measured. In a previous publication [16], the authors showed that the steady-state friction coefficients of as-received and conditioned samples are similar for a given material and are independent of the wear mechanism. This similarity is due to the nature of the oxidation at the pin-disk interface that ultimately develops during wear testing at high temperatures in the ambient air environment of the tribometer. Different steady-state coefficients of friction were measured for as-received Inconel™ 617 [23] at 950 °C and Incoloy™ 800HT at 750 °C [18] in air and impure He environments under a 5N load. The vast majority of material removal due to the wear process occurs during the run-in period. For this reason, plots of steady-state friction coefficients are not shown herein, as the initial coefficients provide the needed insight into the tribological behavior as the samples are experiencing wear.

When considering the exceptional wear resistance provided by the formation of a protective glaze-oxide layer during sliding, such a layer formed more consistently on conditioned alloy 617 compared to conditioned alloy 800HT, confirming the significant role that the mechanical integrity of the oxide and the mechanical integrity of the oxide-base metal interface play in the persistence of the oxide layer under wear conditions. Oxidation rate is also an important consideration, as was seen with the protective oxide that formed on Kolsterised 800HT during temperature ramp-up. Kolsterising® increased the oxidation rate for alloy 800HT more dramatically than that for alloy 617, resulting in the formation of a thick oxide during temperature ramp up that offered protection of the carburized base metal.

5. CONCLUSIONS

For both alloys 800HT and 617, wear resistance was found to be determined by a combination of both the mechanical integrity of a surface oxide (if present) and the hardness of the base alloy. A protective oxide layer reduced wear volumes to negligible levels, and a harder base alloy can arrest the wear process when a protective oxide is either not present or is removed during the initial stage of wear. Initial friction coefficients indicate the degree to which the surface is worn at the beginning of the tribotesting and correlates well with the wear mechanisms. Wear volumes reveal the degree to which the samples become damaged as they reach steady-state sliding and correlate with the hardness of the surface. The order-of-magnitude difference in wear volumes confirms that as-received alloy 617 is more wear resistant than alloy 800HT overall due to its relatively higher hardness at the temperatures investigated in this study. The formation of a glaze-oxide layer can be achieved with an oxide of sufficient mechanical integrity, which is a function of both the quality of the oxide-base metal interface and the applied load. With glaze-oxide-layer formation, wear volumes were below the threshold of the measurement technique. Kolsterising® increased the surface hardness of both alloys, reducing the wear volumes by an order of magnitude on average. Kolsterising also increased the oxidation rate for both alloys and enabled the formation of a glaze-oxide layer on alloy 800HT without a pre-existing oxide. For 800HT, Kolsterising® followed by conditioning produced a weak interface between the external and internal oxides, which caused oxide breakthrough during wear and prevented the formation of a glaze-oxide layer on the samples.

6. ACKNOWLEDGEMENTS

This work was supported by the U.S. Department of Energy (DOE), Nuclear Energy University Program (NEUP) under Award No. DE-NE0008548.

The authors gratefully acknowledge the use of facilities and instrumentation supported by NSF through the University of Wisconsin Materials Research Science and Engineering Center (DMR-1720415).

The authors would also like to acknowledge Dr. Robert Erck, Dr. Dileep Singh, and Dr. Oyelayo Ajayi at Argonne National Laboratory for their expertise and guidance with the use of the high-temperature tribometer.

7. REFERENCES

[1] Davis CB. Implementation of Molten Salt Properties into RELAP5-3D/ATHENA, INEEL/EXT-05-02658, Idaho National Engineering and Environmental Laboratory. 2005.

[2] Wright RN. Kinetics of Gas Reactions and Environmental Degradation in NGNP Helium, INL/EXT-06-11494, Idaho National Laboratory. 2006.

[3] Quadakkers WJ, Schuster H. Thermodynamic and Kinetic Aspects of the Corrosion of High-Temperature Alloys in High-Temperature Gas-Cooled Reactor Helium. Nucl Technol 1984;66:383–91. https://doi.org/10.13182/NT84-A33441.

[4] Cabet C, Terlain A, Lett P, Guétaz L, Gentzbittel J-M. High temperature corrosion of structural materials under gas-cooled reactor helium. Mater Corros 2006;57:147–53. https://doi.org/10.1002/maco.200503901.

[5] Jang C, Lee D, Kim D. Oxidation behaviour of an Alloy 617 in very high-temperature air and helium environments. Int J Press Vessel Pip 2008;85:368–77. https://doi.org/10.1016/j.ijpvp.2007.11.010.

[6] Quadakkers WJ. Corrosion of High Temperature Alloys in the Primary Circuit Helium of High Temperature Gas Cooled Reactors. Part II: Experimental Results. Mater Corros Und Korrosion 1985;36:335–47. https://doi.org/10.1002/maco.19850360802.

[7] Natesan K, Purohit A, Tam S. Materials behavior in HTGR environments 2003.

[8] Lavella M. Contact Properties and Wear Behaviour of Nickel Based Superalloy René 80. Metals (Basel) 2016;6. https://doi.org/10.3390/met6070159.

[9] Tsyntsaru N, Dikusar A, Cesiulis H, Celis JP, Bobanova Z, Sidel'Nikova S, et al. Tribological and corrosive characteristics of electrochemical coatings based on cobalt and iron superalloys. Powder Metall Met Ceram 2009;48:419–28. https://doi.org/10.1007/s11106-009-9150-7.

[10] De Las Heras E, Egidi DA, Corengia P, González-Santamaría D, García-Luis A, Brizuela M, et al. Duplex surface treatment of an AISI 316L stainless steel; microstructure and tribological behaviour. Surf Coatings Technol 2008;202:2945–54. https://doi.org/10.1016/j.surfcoat.2007.10.037.

[11] Hokkirigawa K, Kato K, Li ZZ. The effect of hardness on the transition of the abrasive wear mechanism of steels. Wear 1988;123:241–51. https://doi.org/10.1016/0043-1648(88)90102-0.

[12] Lee BW. Effect of diffusion coatings on the high-temperature properties of nickel-chromium-superalloys. Int J Mod Phys B 2018;32:1840056. https://doi.org/10.1142/S0217979218400568.

[13] Panda RR, Mohantyb DA., Mohanta D. Mechanical and Wear Properties of Carburized Mild Steel Samples. Int J Multidiscip Curr Res 2014;12:109–12. https://doi.org/207ME 207.

[14] Kolsterising® - Bodycote Plc n.d. https://www.bodycote.com/technical-glossary/kolsterising/ (accessed February 13, 2020).

[15] The frequently asked questions of Kolsterising ® - Bodycote blog n.d. http://blog.bodycote.com/2017/06/17/frequently-asked-questions-kolsterising/ (accessed February 13, 2020).

[16] Pauly V, Tesch C, Kern J, Clark M, Grierson D, Singh D, et al. High-temperature tribological behavior of structural materials after conditioning in impure-helium environments for high-temperature gas-cooled reactor applications. J Nucl Mater 2019;522:311–23. https://doi.org/10.1016/j.jnucmat.2019.05.025.

[17] Baryshev S V., Erck RA, Moore JF, Zinovev A V., Tripa CE, Veryovkin I V. Characterization of surface modifications by white light interferometry: applications in ion sputtering, laser ablation, and tribology experiments. J Vis Exp 2013:e50260. https://doi.org/10.3791/50260.

[18] Rahman S, Ding J, Beheshti A, Zhang X, Polycarpou AA. Tribology of incoloy 800HT for nuclear reactors under helium environment at elevated temperatures. Wear 2019:1–11. https://doi.org/10.1016/j.wear.2019.203022.

[19] Collins SR, Williams PC, Marx S V, Company S, Heuer A, Ernst F, et al. Low-Temperature Carburization of Austenitic Stainless Steels. ASM Handbo. ASM International; 2014.

[20] Cao Y, Ernst F, Michal GM. Colossal carbon supersaturation in austenitic stainless steels carburized at low temperature. Acta Mater 2003;51:4171–81. https://doi.org/10.1016/S1359-6454(03)00235-0.

[21] Tan L, Rakotojaona L, Allen TR, Nanstad RK, Busby JT. Microstructure optimization of austenitic Alloy 800H (Fe-21Cr-32Ni). Mater Sci Eng A 2011;528:2755–61. https://doi.org/10.1016/j.msea.2010.12.052.

[22] Rahman S, Polychronopoulou K, Polycarpou AA. Tribochemistry of inconel 617 during sliding contact at 950 C under helium environment for nuclear reactors. J Nucl Mater 2019;521:21–30. https://doi.org/10.1016/j.jnucmat.2019.04.032.

[23] Rahman S, Ding J, Beheshti A, Zhang X, Polycarpou AA. Helium Tribology of Inconel 617 at Elevated Temperatures up to 950°C: Parametric Study. Nucl Sci Eng 2019;193:998–1012. https://doi.org/10.1080/00295639.2019.1582315.

[24] He N, Li H, Ji L, Liu X, Zhou H, Chen J. Reusable chromium oxide coating with lubricating behavior from 25 to 1000 °C due to a self-assembled mesh-like surface structure. Surf Coatings Technol 2017;321:300–8. https://doi.org/10.1016/j.surfcoat.2016.12.082.

[25] Salari S, Rahman MS, Polycarpou AA, Beheshti A. Elevated temperature mechanical properties of Inconel 617 surface oxide using nanoindentation. Mater Sci Eng A 2020;788:139539. https://doi.org/10.1016/j.msea.2020.139539.

[26] Stott FH, Lin DS, Wood GC. The structure and mechanism of formation of the “glaze” oxide layers produced on Nickel-based alloys during wear at high temperatures. Corros Sci 1973;13:449–69.

[27] Sharghi-Moshtaghin R, Kahn H, Ge Y, Gu X, Martin FJ, Natishan PM, et al. Low-temperature carburization of the ni-base superalloy IN718: Improvements in surface hardness and crevice corrosion resistance. Metall Mater Trans A Phys Metall Mater Sci 2010;41:2022–32. https://doi.org/10.1007/s11661-010-0299-y.

[28] Rahman S, Ding J, Beheshti A, Zhang X, Polycarpou AA. Elevated temperature tribology of Ni alloys under helium environment for nuclear reactor applications 2018. https://doi.org/10.1016/j.triboint.2018.03.021.

[29] Ahmadi A, Sadeghi F, Shaffer S. In-situ friction and fretting wear measurements of Inconel 617 at elevated temperatures. Wear 2018;410–411:110–8. https://doi.org/10.1016/j.wear.2018.06.007.

[30] Scherge M, Shakhvorostov D, Pöhlmann K. Fundamental wear mechanism of metals. Wear 2003;255:395–400. https://doi.org/10.1016/S0043-1648(03)00273-4.

[31] Eyre TS. Wear characteristics of metals. Tribol Int 1976;9:203–12. https://doi.org/10.1016/0301-679X(76)90077-3.

[32] So H, Yu DS, Chuang CY. Formation and wear mechanism of tribo-oxides and the regime of oxidational wear of steel. Wear 2002;253:1004–15. https://doi.org/10.1016/S0043-1648(02)00230-2.

[33] Lim SC. Recent developments in wear-mechanism maps. Tribol Int 1998;31:87–97. https://doi.org/10.1016/S0301-679X(98)00011-5.

[34] Lim SC. The relevance of wear-mechanism maps to mild-oxidational wear. Tribol Int 2002;35:717–23. https://doi.org/10.1016/S0301-679X(02)00033-6.